Reversible Lignin-Containing Networks Using Diels-Alder Chemistry

Thys, Marlies; Brancart, Joost; Van Assche, Guy; Vendamme, Richard; Van den Brande, Niko

Published in:
Macromolecules

DOI:
10.1021/acs.macromol.1c01693

Publication date:
2021

Reversible lignin-containing networks using Diels-Alder chemistry

Marlies Thys[1,2], Joost Brancart[1], Guy Van Assche[1], Richard Vendamme[2], Niko Van den Brande[1]**

[1] Physical Chemistry and Polymer Science (FYSC), Vrije Universiteit Brussel (VUB), Pleinlaan 2, 1050 Brussels, Belgium

[2] Flemish Institute for Technological Research (VITO), Boeretang 200, 2400 Mol, Belgium

For Table of Contents use only:

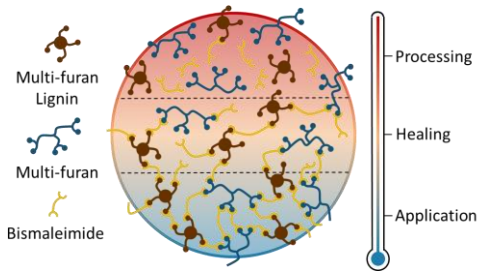

ABSTRACT

The development of bio-based polymers displaying promising end-of-life opportunities would have an immense impact on the polymer industry, but has remained largely unexplored. Therefore, in this work, self-healing bio-aromatic networks with lignin contents up to 29 wt% were designed based on the thermo-reversible Diels-Alder reaction. The networks were developed by reacting a furan-functionalized solvent-extracted lignin and a furan-bearing polyether (F5000) with a bismaleimide (DPBM). The obtained networks were nanophase-separated between a flexible F5000-rich phase and a rigid lignin-rich phase, which was evidenced by (modulated temperature) differential scanning calorimetry ((MT)DSC) and small angle x-ray scattering (SAXS). Partially due to the phase-separation, improved mechanical properties were obtained, including a higher Young's modulus and improved toughness. In addition, the thermal stability of the networks significantly increased due to the addition of lignin. Besides the thermomechanical improvement, the networks showed promising stress-relaxation, creep resistance, healing and reprocessability. A macroscopic healing efficiency of 62 % of the toughness was obtained. Moreover, the networks were completely resoluble, which allows for promising recycling possibilities.

INTRODUCTION

The interest in bio-based polymers as an alternative route to develop commonly used plastics is growing intensively. This growth has been mainly attributed to the increasing production capacity of polylactic acid (PLA), starch-containing polymers, polybutylene adipate terephthalate (PBAT), polyhydroxyalkanoates (PHA), and epoxy resins.[1] Currently, glucose intermediates derived from starch, sugars, and lignocellulose predominantly contribute to this biopolymer production, being transformed into a range of different monomer building blocks.[1] However, glucose does not possess the key aromatic structures required for the development of aromatic-rich polymers displaying outstanding thermal and mechanical properties. Moreover, efficient ways to transform aliphatic bio-based feedstock into aromatic-functional materials are still extremely challenging.[2] It is therefore not surprising that the synthesis of (semi)aromatic polymers derived from renewable resources is attracting tremendous interest from industry.

Lignin is an aromatic amorphous polymer that is industrially separated from wood as a biogenic residue of the pulping process. Besides its known application as a fuel, the aromatic nature of lignin makes it a promising candidate to be used in higher value-added applications, such as polymers, resins, and composite materials.[3] Despite the increasing scientific effort in the development of lignin-containing materials, the use of lignin as a feedstock for polymers and composites has had only limited success so far. This is because the 3D structure of lignin is complex and its reactivity limited, rendering its incorporation into synthetic polymers and formulations quite difficult. As a result, lignin fractionation techniques such as membrane filtration[4–6] and solvent extraction[7–10] have gained considerable attention in recent polymer

literature, showing successful incorporation of the fractionated lignin into epoxy resins[11,12], polyurethanes[13–15], coatings[16,17], and adhesives[18].

However, the resulting materials are often limited in their recycling and reprocessing opportunities due to their permanent crosslinked structure. Consequently, an important trend in polymer science, especially regarding thermosets, is the development of "smart" materials displaying adaptive properties, such as self-healing, or the possibility for the material to be reprocessed or re-shaped.[19–22] This adaptivity can be realized by the incorporation of reversible chemical bonds in the polymer structure, achieved for example via the thermoreversible Diels-Alder (DA) equilibrium reaction. This [4+2] cycloaddition between a diene and a dienophile can form two thermoreversible Diels-Alder stereoisomers; the *endo* adduct, which is kinetically favored, and the *exo* adduct, which is thermodynamically favored (Scheme 1). Increasing the temperature will shift the equilibrium towards the dissociation of the adducts into the diene and dienophile, and vice versa upon cooling. A well-described Diels-Alder combination is furan and maleimide, as the diene and dienophile respectively. This combination is thermoreversible in a temperature window typically between 80 °C and 130 °C and showed effective healing in several thermosetting materials.[23–28]

Scheme 1. Diels-Alder reversible equilibrium reaction between furan and maleimide, showing the *endo* and the *exo* stereoisomeric adducts

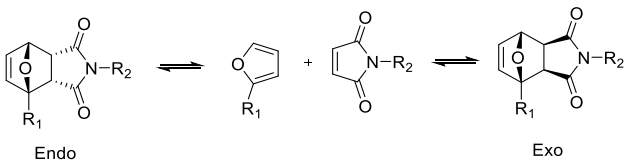

In this work, bio-aromatic self-healing networks were developed based on reversible DA bonds, introduced by reacting a furan-functionalized lignin with a bismaleimide. The addition of furan-functionalized lignin into DA formulations was earlier described in reversible hydrogels,[29,30] but remained largely unexplored in bulk polymers. To the authors' knowledge, Habibi *et al*. were the first to describe a lignin-based self-healable network based on maleimide-modified soda lignin linked to different multifunctional furan linkers.[31] Their material contained up to 30 wt% lignin and showed promising healing and reprocessing behavior. However, the rather weak mechanical properties merit further investigation. Here, we describe the development of processable high modulus networks using ethyl methyl ketone (EMK) fractionated Kraft lignin modified with furan-bearing groups. These lignin fractions were integrated into a furfurylated polyether-bismaleimide self-healing network to obtain the resultant thermoreversible bio-aromatic networks. The networks were characterized using thermal analysis, including thermogravimetric analysis (TGA) and (modulated temperature) differential scanning calorimetry ((MT)DSC) to investigate the thermal stability of the networks and the thermal transitions, such as the glass transition temperature (T_g), respectively. Information about the glass transition allows the determination of an operating temperature window for healing and processing experiments. In addition, to investigate the effect of lignin incorporation on the modulus the (thermo)mechanical properties were analyzed using dynamic mechanical analysis (DMA) and tensile measurements. Rheometric analysis was performed to characterize the stress relaxation and creep behavior of the networks. Finally, the macroscopic healing and reprocessing of the networks was investigated.

Materials and methods

Materials. Jeffamine T5000, with an average molar mass of 5649 g mol^{-1}, was supplied by Huntsman (Belgium). Furfuryl glycidyl ether (FGE), 1,1′-(methylenedi-4,1-phenylene)bismaleimide (DPBM), hydroquinone (HQ), chloroform, ethyl methyl ketone (EMK), and sodium hydroxide (NaOH) were all purchased from Sigma Aldrich. Lignoboost® softwood Kraft lignin (pine) was provided by Innventia Institute. All products (Scheme 2) were used as received.

Scheme 2. Molecular structures of the starting reagents used in the bio-aromatic reversible networks: (a) Simplified structure of Kraft lignin, (b) Jeffamine T5000 with (x+y+z) ≈ 85, (c) Furfuryl glycidyl ether (FGE), and (d) Crystalline bismaleimide DPBM

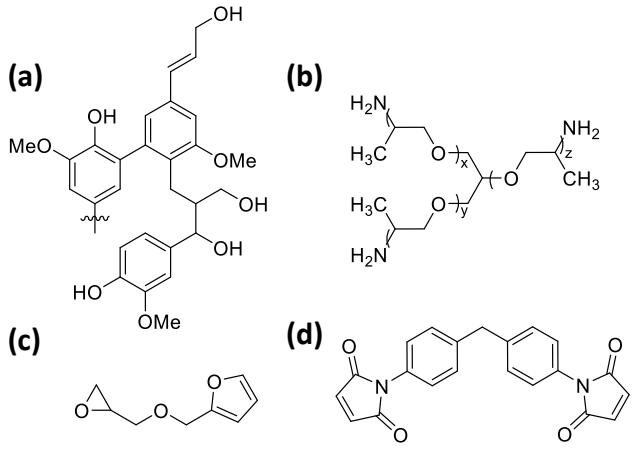

Preparation of reversible DA networks. *Synthesis of F5000 (furfurylated Jeffamine).* Trifunctional Jeffamine T5000 was functionalized with furan moieties using the irreversible epoxy-amine reaction with monofunctional furfuryl glycidyl ether as described in literature.[24,32,33]

The reaction was stoichiometrically performed without the use of a solvent or catalyst. The mixture was allowed to stir for 7 days at 60 °C followed by 2 days at 90 °C to complete the reaction. The final F5000 structure was confirmed by ^{1}H-NMR, displaying a furan functionality of 6.[33]

Synthesis of F-KL$_{EMK}$ (furfurylated lignin). Kraft lignin (KL) functionalization was performed in a two-step procedure. In the first step, KL was dissolved in ethyl methyl ketone (EMK, 15 % m/v) and stirred overnight at ambient temperature. The solution was then filtered over a Büchner filter and the filtrate was dried by rotary evaporation. The obtained powder was further dried in a vacuum oven overnight at 40 °C, resulting in the desired EMK extracted lignin fraction (KL$_{EMK}$) with a yield of 45 %. In the second step, KL$_{EMK}$ was dissolved in an aqueous NaOH solution (1 eq NaOH towards the acidic groups of KL$_{EMK}$ (phenolic OH and COOH)) as described in literature.[29] After 1 h of stirring, furfuryl glycidyl ether was added (1.25 eq to the KL$_{EMK}$ phenolic hydroxyl groups) and the reaction mixture was allowed to stir overnight at 50 °C. After cooling down to ambient temperature, the mixture was acidified to pH 2 using a 1 % (v/v) HCl solution. The precipitated solids were washed 3 times with acidified water of pH 2 and subsequently vacuum-dried at 40 °C overnight, to quantitively yield F-KL$_{EMK}$ with an average furan functionality of 4 (calculations of the F-KL$_{EMK}$ functionality can be found in the supporting information).

Formulation of reference DA network. The reference Diels-Alder network (DA-L0) was developed by dissolving F5000 (1.99 mmol furan groups, 2.14 g), DPBM (1.99 mmol maleimides, 0.36 g), and HQ (1 wt% to DPBM) in chloroform (diluted to 20 wt%). The mixture was stirred for 24 h at ambient temperature and was subsequently degassed for 2 h. The homogeneous solution was then cast in a Teflon mold covered with a semi-perforated box to allow slow evaporation of chloroform for 24 h at ambient temperature. The obtained networks were stored for 2 weeks at 30 °C prior to analysis.

Formulation of lignin-DA networks. The lignin-containing networks were developed using the same procedure as the reference network. To increase the lignin content, the F-KL_{EMK}/F5000 molar ratio was changed, while keeping the furan/maleimide ratio, given by ($n_{F\text{-}KL_{EMK}}$ + n_{F5000})/n_{DPBM} , at unity. This led to the development of DA-L40, DA-L50, and DA-L60, using the furan and maleimide concentrations shown in table 2. The mixtures were stirred for 6 h and were post-treated in an oven for 3 h at 80 °C to assure complete equilibrium conditions.

Healing procedure. All samples were healed following an optimized temperature program. The reference network (DA-L0) was healed for 45 min at 85 °C followed by gradually cooling of 5 K per 30 min until 40 °C. The lignin-containing networks DA-L40, DA-L50, and DA-L60 were healed for 45 min at 120 °C, 125 °C, and 130 °C, respectively, followed by a gradual cooling at 1 K min^{-1} to 85 °C, followed by a slow cooling at 5 K per 30 min to 40 °C. All samples were subsequently kept overnight in an oven at 40 °C and stored for at least two days at ambient temperature prior to further analysis.

Characterization methods. *Thermogravimetric analysis,* TGA thermograms were measured on a TA Instruments TGA Q5000IR. The measurements were performed under an air or nitrogen flow rate of 25 mL min^{-1} depending on whether an oxidative or inert environment was required. A heating rate of 20 °C min^{-1} was applied from 50 °C to 600 °C.

(Modulated temperature) differential scanning calorimetry, (MT)DSC was performed on a TA Instruments Discovery DSC 250 equipped with a refrigerated cooling system (RCS) that allows cooling to -90 °C. The samples were measured in Tzero pans with perforated Tzero hermetic lids to allow a nitrogen atmosphere around the sample. DSC thermograms were recorded with a heating rate of 20 °C min^{-1}. MTDSC thermograms were recorded with a heating rate of 3 K min^{-1}, a period

of 60 s, and a temperature amplitude of 0.5 °C. Only experimental data obtained from the second heating step will be reported.

Dynamic mechanical analysis, The viscoelastic properties were measured on a Discovery DMA 850 from TA instruments. The DMA was equipped with a gas cooling accessory (GCA) to allow cooling below -100 °C. Measurements were performed in tension mode using a film tension clamp. Each material was measured 3 times, with sample dimensions of ca. 0.5 mm thickness, a width of 7.0 mm, and a length of 7 mm. The estimation of the experimental error on the DMA results is described in the supporting information.

Dynamic rheometry, Stress relaxation, creep resistance and melt viscosity experiments were performed on a Discovery HR-2 hybrid rheometer of TA Instruments. The instrument was equipped with a forced convection oven (FCO) surrounding the 8 mm plate-plate configuration. For stress relaxation, a strain of 1 % was applied with an axial force of 2 N. Stress relaxation data of DA-L0 and DA-L40 were smoothed using the Savitzky-Golay method using a polynomial order of 2 and a window size of 10 points. Creep resistance experiments were performed with an alternating stress of 0 Pa and 3000 Pa, and an axial force of 5 N. Melt viscosity was measured with a steady shear rate of 1 s^{-1} to 10 s^{-1}. In all measurements the sample disks had a diameter of 8 mm and a thickness of ca. 0.5 mm.

Tensile testing, Tensile analysis of the reversible networks were conducted on an Instron 6800 Single column tensile tester using pneumatic clamps. 5 replicates were measured for each sample, using sample dimensions of 22 x 5 x 0.6-0.7 mm. The tests were performed at ambient temperature and 50–60% relative humidity. The crosshead speed was 5 mm min^{-1}. The estimation of the experimental error on the tensile testing results is described in the supporting information.

RESULTS AND DISCUSSION

Fractionation and modification of lignin. Kraft lignin (KL) is highly incompatible with most solvents and reactants, mainly due to its high molar mass. Therefore, an EMK (ethyl methyl ketone) solvent extraction was performed to solubilize exclusively the lower molar mass fractions, resulting in a more compatible and reactive lignin (KL_{EMK}).[8] The properties of KL_{EMK} compared to KL are listed in table 1 and show a clear reduction in molar mass (M_n and M_w), dispersity ($Đ$), and glass transition (T_g) as a direct result of the extraction conditions. In addition, a significant decrease in aliphatic hydroxyl groups (Aliph-OH) combined with a small increase in phenolic hydroxyl groups (Phen-OH) was observed. Similar observations were previously reported and were linked to the chemistry of the Kraft process.[9,34] In this process, the native lignin is degraded into smaller fragments, leading to the formation of Phen-OH and the cleavage of aliph-OH, resulting in a lower aliph-OH content in the lower molar mass fractions.[35]

Table 1. Molecular parameters and thermal properties of lignin samples

	M_w (g mol^{-1})[a]	M_n (g mol^{-1})[a]	$Đ$[a]	Aliph-OH (mmol g^{-1})[b]	Phen-OH (mmol g^{-1})[b]	COOH (mmol g^{-1})[b]	T_g (°C)[c]
KL	5200	1420	3.66	1.95	4.32	0.43	124
KL_{EMK}	2100	1010	2.09	1.25	4.55	0.54	63
F-KL_{EMK}	3360	1710	2.00	3.46	0.33	0.35	41

Weight and number average molar mass, M_w and M_n, polydispersity index ($Đ = M_w/M_n$), mass-based concentration of aliphatic hydroxyl (Aliph-OH), phenolic hydroxyl (Phen-OH), and carboxylic acid (COOH) groups, and the glass transition temperature T_g; *Determined by [a]GPC, [b]31P-NMR (Figure S1) and [c]DSC (Figure S2)*

KL_{EMK} was subsequently functionalized with furan moieties to participate in the reversible furan-maleimide reaction. This modification was performed by reaction between the phenolic

hydroxyl groups of KL_{EMK} and the epoxide of furfuryl glycidyl ether (FGE) in basic conditions (Scheme 3). The formation of the irreversible ether bond resulted in a decrease of aromatic OH-groups, combined with an increase of aliphatic OH-groups due to the opening of the epoxides. Both events were confirmed by ^{31}P-NMR and are quantified in Table 1 as F-KL_{EMK}. FT-IR spectroscopy supported the successful conversion, showing characteristic peaks of the furan ring at 740 cm^{-1} and 600 cm^{-1} (Figure S3b). The ether bonds originating from the FGE linker were also clearly visible at 1150 cm^{-1}. The significant drop in T_g was not expected, but it was attributed to the disruption of intermolecular hydrogen bonds between the lignin molecules by the FGE linker. This assumption is supported by FT-IR, where the shoulder at 3500 cm^{-1} (indicating intermolecular OH bonding) disappeared for F-KL_{EMK} (Figure S3a).[36]

Scheme 3. Reaction of KL_{EMK} with FGE in basic conditions for the formation of F-KL_{EMK}

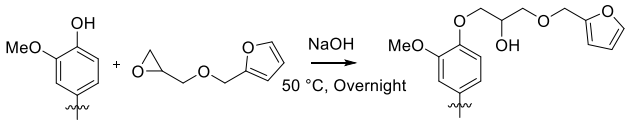

Development of lignin-based DA networks. Reversible Diels-Alder (DA) networks based on a furan-functionalized Jeffamine Fx (x ranging from 230 to 5000) and crystalline DPBM have been extensively studied in our group[24,32,33,37]. In this work, due to the rigid nature of lignin, only Fx-DPBM combinations with the desired elastomeric properties were considered to ensure optimal mobility in the reversible lignin-based networks. Consequently, the reference network was based on the hexafunctional F5000 - bifunctional DPBM combination in which F-KL_{EMK} was integrated to increasing extents. The lignin-based DA networks were developed with a furan to maleimide ratio of one (F/M = 1). While keeping the F/M ratio at unity, increasing amounts of F-KL_{EMK} were

integrated into the network formulations, as can be seen in table 2. The furan compounds F5000 and F-KL_{EMK} possess different furan functionalities, being 6 and 4, respectively (calculations of the F-KL_{EMK} functionality can be found in the supporting information), and different functional weights (molar mass per functionality). Due to the lower functional weight of the F-KL_{EMK} compared to the F5000, maleimide and furan concentrations increase with increasing lignin content. Consequently, the crosslink density of the networks increases with higher lignin contents. The networks were developed by casting homogeneous chloroform solutions based on F5000, DPBM, and F-KL_{EMK} in Teflon molds covered with a semi-perforated box, to allow slow chloroform evaporation for 24 h, and were subsequently post-treated for 3h in an oven of 80 °C. The reference network (DA-L0) was obtained as a yellow transparent elastomeric network, whereas the lignin-containing networks (DA-L40, DA-L50, and DA-L60) were obtained as dark-brown transparent elastomeric networks. The brown color intensified with increasing lignin content (Figure 1).

Table 2. Experimental values for the development of lignin-containing DA networks

	F-KL_{EMK}/F5000	**$[M]_{DPBM}$ (mol kg^{-1})**	**$[F]_{F5000}$ (mol kg^{-1})**	**$[F]_{F\text{-}KL_{EMK}}$ (mol kg^{-1})**	**wt% F-KL_{EMK}**
DA-L0	0/100	0.774	0.774	0	0
DA-L40	40/60	0.982	0.589	0.393	16.6
DA-L50	50/50	1.053	0.526	0.526	22.2
DA-L60	60/40	1.134	0.454	0.680	28.7

Ratio of mol fractions of F-KL_{EMK}/F5000, maleimide concentration of DPBM ($[M]_{DPBM}$), furan concentration of F5000 ($[F]_{F5000}$), furan concentration of F-KL_{EMK} ($[F]_{F\text{-}KL_{EMK}}$), and mass fraction of F-KL_{EMK}

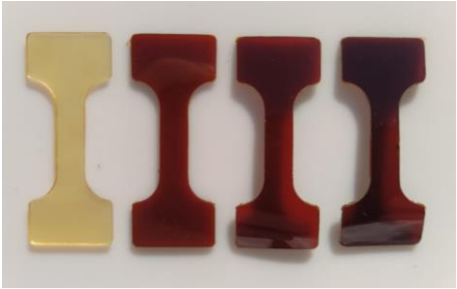

Figure 1. Pictures of the developed networks; from left to right: DA-L0, DA-L40, DA-L50 and DA-L60.

Thermal characterization of lignin-DA networks. The thermal behavior is of great importance during the development of self-healing networks as it determines the operating temperature window for self-healing and reprocessing operations. Thermogravimetric analysis (TGA) was performed to investigate the effect of increasing lignin content on the thermal stability of the developed networks in nitrogen (Figure 2a) and air (Figure 2b). Initially, all thermograms show a similar decreasing trend between 150 °C and 230 °C, indicating a weight loss of less than 2%, related to small quantities of trapped chloroform or small molecules in the network structure. In air atmosphere, the reference network (DA-L0) starts degrading from 250 °C onwards, indicating some sensitivity towards oxidation (Figure 2b). This observation is supported by the TGA thermograms of the materials under nitrogen atmosphere, where no significant difference in thermal stability was observed between the reference and lignin-containing networks (Figure 2a). The addition of lignin increased the degradation temperature by an average of 100 °C (table 4). This improvement can be assigned to the aromatic nature of lignin and partially by the presence of remaining phenolic OH groups (roughly 11%).[38] The aromaticity of lignin and specifically the aromatic char could act as a protective layer for the polyether backbone chain resulting in an increase in thermal degradation temperature.[39] In addition, the remaining phenolic OH groups

might also partially contribute to this improved thermal stability by acting as inhibitors for free radical reactions involved in oxidative degradation[40], which might also explain their anti-oxidative activity.[38] Additionally, both thermograms also show an increase in ash content with increasing lignin concentration, which is mostly related to carbon-carbon aromatic residues. These increasing amounts of char could be of special interest in flame-retardance applications.[41]

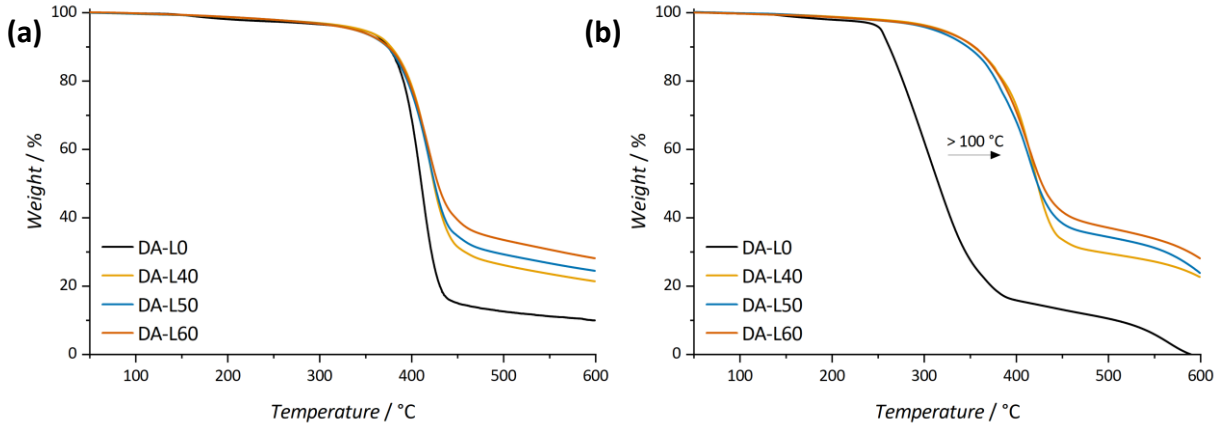

Figure 2. Thermal stability analysis of DA-L0, DA-L40, DA-L50, and DA-L60 by TGA performed at a heating rate of 20 K min^{-1} (a) under nitrogen purge and (b) under air purge.

DSC thermograms were measured for DA-L0, DA-L40, DA-L50, and DA-L60 (Figure 3) and show multiple thermal transitions above 50 °C. These are attributed to the formation of two different stereoisomers of the DA-cycloadducts, the *endo* and *exo* isomer (Zoom in Figure 3). All networks show a first exothermic peak, representing the association of both adducts, followed by two endothermic peaks. The first endothermic peak indicates the endothermic dissociation of the *endo* adduct, combined with the exothermic continued association of the *exo* adduct. The second peak represents the endothermic dissociation of the thermodynamically more stable *exo* adduct.[42] These thermal transitions are more pronounced for the reference DA-L0 network and

become less distinguishable for the lignin-containing samples. On first impression this might be attributed to a higher exo/endo adduct ratio, but it will be shown that this is not the case.

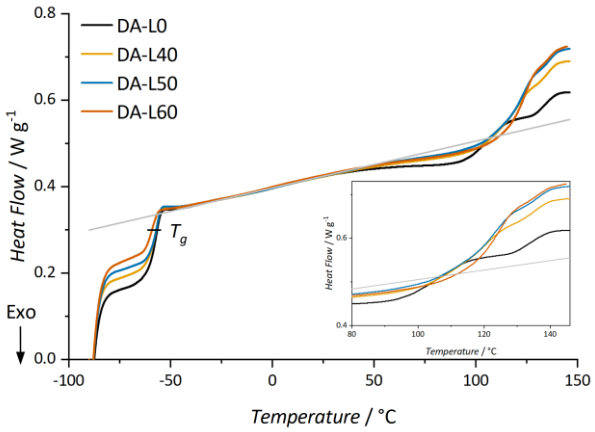

Figure 3. DSC thermogram of the second heating cycle at 20 K min^{-1} with a zoom of 80 °C to 147 °C. The thermograms were shifted to overlap between -30 °C to 30 °C.

In addition to the association and dissociation peaks, a clear glass transition (T_g) is visible at -58 °C, independent of the lignin concentration, which matches well with the T_g of -61 °C for the pure F5000. However, with increasing lignin content a marked decrease in the height of the heat capacity increase at the T_g (ΔC_p) is observed. This T_g independence of the lignin content, combined with a decrease in ΔC_p and the optically translucent character of the network films, suggests that phase separation is occurring between the flexible F5000 linker and the rigid lignin linker on a sub-micron scale. However, if phase separation between a lignin-poor and lignin-rich phase is occurring, a second T_g originating from the lignin-containing phase is expected though not observed in the thermograms. Therefore, modulated temperature DSC (MTDSC) measurements were performed, as this technique in some cases allows for the deconvolution of overlapping thermal transitions; in this case to deconvolute a T_g from the overlapping DA association and

dissociation peaks. In figure 4, the reversing heat capacity shows a first T_g at -61 °C for all networks and a second T_g at 127 °C, which is absent in the reference DA-L0 sample. Therefore, the T_g's at -61 °C and 127 °C can be assigned to a flexible F5000-phase and a rigid lignin-containing phase, respectively. Moreover, it becomes clear that the presence of a second T_g underneath the association and dissociation peaks is largely responsible for the difference in the shape of the dissociation endotherm between the reference and lignin containing samples. SAXS measurements confirmed the presence of a phase-separated structure for all lignin networks with a clear q-peak at 0.42 nm^{-1} corresponding to a domain spacing of 14-15 nm (Figure S4). In addition, the tan (δ) peaks, measured in DMA (Figure 5c), recover to the level observed before the glass transition, indicating a relatively sharp phase separation and the absence of an extensive interphase between the low-T_g and the high-T_g phase. Only for DA-L60, the tan (δ) signal suggests a gradual transition between the two phases, typical of incomplete phase separation and the formation of an interphase with a composition gradient. The non-reversing heat flow of the MTDSC thermograms shows the association and dissociation peaks of the DA-adducts. However, it has to be noted that this thermogram lacks the first exothermic peak (association of *endo* adducts). This is related to the previous slow cooling rate used in MTDSC (3 K min^{-1}), which promotes the formation of the more stable *exo* isomer, whereas the higher cooling rate used in DSC (20 K min^{-1}) allows less time for association during cooling and, hence, the formation of more *endo* adduct during storage at lower temperatures. In addition, the lower heating rates in MTDSC result in a shift of the retro-DA reaction to lower temperatures.

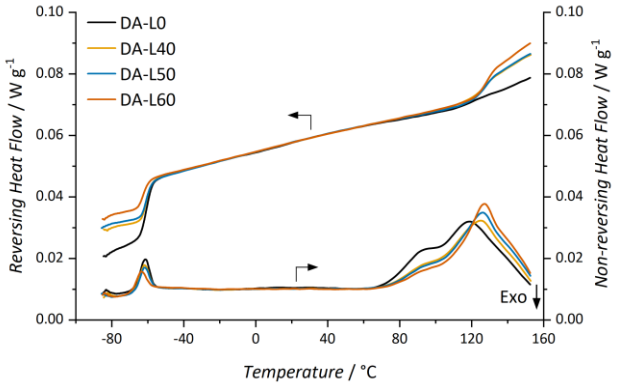

Figure 4. MTDSC thermograms for DA-L0, DA-L40, DA-L50, and DA-L60 measured at a heating rate of 3 K min^{-1}. The thermograms were shifted to superimpose overlap between -30 °C and 30 °C.

As the lignin-containing networks are phase-separated between a flexible (low T_g) and a rigid (high T_g) phase, it is important to know the distribution of the bismaleimide linker (DPBM) in both phases, as it will drastically influence the healing efficiencies at a certain temperature. In theory, the enthalpic driving force for Diels-Alder association is higher than the driving force for phase separation, which insinuates that the DPBM should be equimolarly spread over the two phases.[43] Moreover, the long mixing times allow the reaction to proceed already to a great extent during continuous homogenization. To confirm this statement, a theoretical heat capacity change ΔC_p for DA-L40, DA-L50, and DA-L60 was calculated for each of the constituting phases (ΔC_{p1} for the flexible phase and ΔC_{p2} for the rigid phase). For the pure phases, ΔC_{p1} for a 100 % F5000-DPBM phase corresponds to 0.33 J g^{-1} K^{-1}, as was measured by MTDSC for DA-L0, while ΔC_{p2} of a 100 % lignin-DPBM sample measured by MTDSC corresponds to 0.40 J g^{-1} K^{-1} (Figure S5 and Table 3). To calculate the theoretical heat capacities, the weight percentages of each phase ($wt\%_{F5000+DPBM}$ or $wt\%_{lignin+DPBM}$) were multiplied with the ΔC_p of the corresponding pure phase. The theoretical ΔC_{p1} and ΔC_{p2} values correlated closely to the measured ΔC_p values of the

networks. The small deviations observed can be related to the presence of mixed (inter)phases (Table 3).

Table 3. Calculation for the assumption that DPBM is equimolarly spread over both phases

		DA-L0	DA-L40	DA-L50	DA-L60	DA-L100
Weight % of each phase (assuming an equimolar distribution of DPBM)						
F5000 + DPBM	wt%	**100**	76	68	58	**0**
Lignin + DPBM	wt%	**0**	24	32	42	**100**
Measured ΔC_{p1} and ΔC_{p2} (ΔC_{p1}= F5000 + DPBM phase and ΔC_{p2} = Lignin + DPBM phase)						
ΔC_{p1}	J g^{-1} K^{-1}	**0.33**	0.24	0.23	0.17	**0**
ΔC_{p2}	J g^{-1} K^{-1}	**0**	0.08	0.11	0.14	**0.40**
Theoretical ΔC_{p1} and ΔC_{p2}						
ΔC_{p1}	J g^{-1} K^{-1}		0.25	0.22	0.19	
ΔC_{p2}	J g^{-1} K^{-1}		0.10	0.13	0.17	

Thermomechanical characterization of lignin-DA networks. Dynamic mechanical analysis (DMA) was performed on all networks to investigate the viscoelastic behavior of the networks. The storage modulus (*E'*) of DA-L0, DA-L40, DA-L50, and DA-L60 at 25 °C was found to be 8 MPa, 17 MPa, 38 MPa, and 186 MPa, respectively (Figure 5a and Table 4). Increasing the lignin content had thus a significant effect on the stiffness of the networks, mainly attributed to the increasing aromaticity and crosslink density. The loss modulus (*E"*) shows a clear maximum at -58 °C, indicating the T_g of the flexible phase and supporting the previous reported DSC data (Figure 5b). Upon heating above the first T_g, both *E'* and *E"* proceed to a rubbery plateau. However, the rubbery plateau for DA-L0 is not constant, but rather gradually decreases with increasing temperature. This gradual decrease is attributed to the shifting of the DA equilibrium towards the DA adduct dissociation, resulting in a decrease in crosslink density and hence in *E'*. This phenomenon is more suppressed in DA-L40, DA-L50, and DA-L60, most probably due to the phase-separated network structure. Therefore, the stiffness is less influenced by temperature for the lignin-containing samples within this rubbery plateau temperature region. This is especially beneficial for application purposes, as the mechanical properties of the lignin-containing networks stay roughly constant over a relatively broad temperature range. Moreover, the mechanical properties can be easily tuned by altering the lignin concentration.

The stress-strain diagrams of the DA-L0, DA-L40, DA-L50, and DA-L60 networks measured at ambient temperature are shown in figure 5d. A substantially higher Young's modulus was obtained with increasing lignin content, ranging from 12.6 MPa for DA-L0 to 425 MPa for DA-L60 (Table 4). In addition, the stress at break increased from 2.8 MPa to 19.8 MPa. These observations are directly related to the increasing lignin-rigid phase in the phase-separated structure, combined with the decrease of the flexible F5000 phase. However, the strain at break

remained comparable (35-52 %) between DA-L40, DA-L50, and DA-L60. This indicates that the F5000-rich phase has an important contribution to this relatively high strain at break as this low T_g-phase is mobile at ambient temperature, and possibly that this phase is continuous, with the more rigid phase being dispersed in it. The toughness of the material increased significantly with increasing lignin content: from 1.13 kJ m^{-3} to 6.22 kJ m^{-3} for DA-L0 and DA-L60, respectively. The phase-separated structure of these DA networks has thus a positive influence on the overall strength of the material.

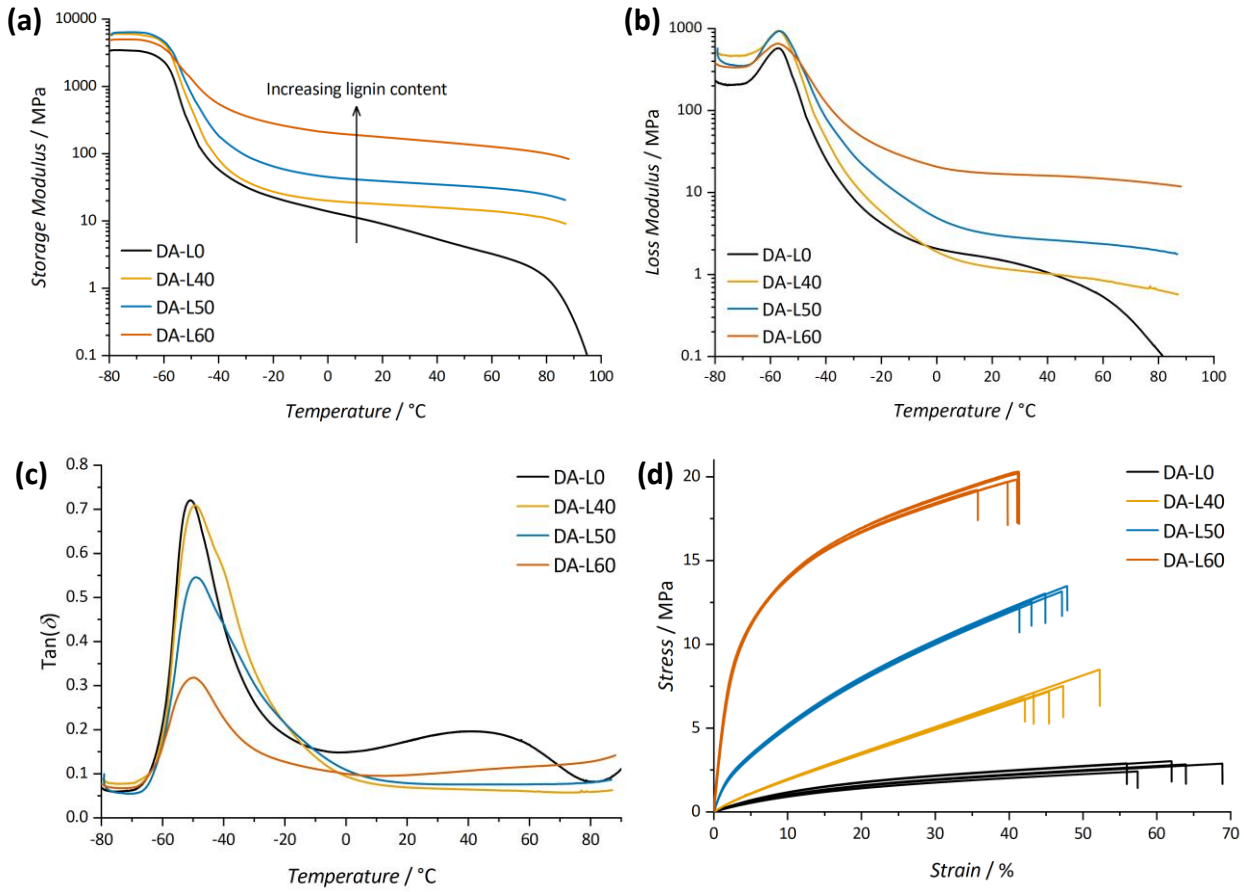

Figure 5. DMA and tensile measurements of DA-L0, DA-L40, DA-L50, and DA-L60; a) Storage modulus, b) loss modulus, c) tan (δ) and d) stress-strain diagram.

Table 4. Thermal and mechanical analysis data of the developed DA networks measured with TGA, (MT)DSC, DMA, and tensile testing

		DA-L0	DA-L40	DA-L50	DA-L60
Thermal degradation: 20 K min^{-1}, T_{d5} = 5wt% loss, T_{deg} = main degradation peak in air atmosphere					
T_{d5}	°C	253	315	310	316
T_{deg}	°C	307	418	415	414
Glass transition: MTDSC (3 K min^{-1}), DMA (2 K min^{-1})					
T_{g1} (MTDSC)	°C	-61	-61	-61	-62
ΔC_{p1}	J g^{-1} K^{-1}	0.33	0.24	0.23	0.17
T_{g2} (MTDSC)	°C	/	127	127	128
ΔC_{p2}	J g^{-1} K^{-1}	/	0.08	0.11	0.14
T_{g1} (DMA)	°C	-59	-57	-58	-58
Viscoelastic behavior at 25 °C					
Storage Modulus (*E'*)	MPa	8.5 ± 0.4	18 ± 1	38 ± 2	186 ± 8
Loss Modulus (*E''*)	MPa	1.5 ± 0.1	1.2 ± 0.1	3.1 ± 0.3	20 ± 2
Phase Angle	°	10 ± 1	4.1 ± 0.3	4.7 ± 0.4	5.9 ± 0.5
Tensile properties					
Young's Modulus	MPa	13 ± 1	20 ± 1	83 ± 4	425 ± 21
Stress at break	MPa	2.8 ± 0.1	7.4 ± 0.3	13 ± 1	20 ± 1
Strain at break	%	62 ± 3	46 ± 3	45 ± 2	40 ± 2
Toughness	kJ m^{-3}	1.1 ± 0.1	1.8 ± 0.2	3.6 ± 0.3	6.2 ± 0.6

Stress relaxation behavior of lignin-based network films. Stress-relaxation experiments were performed within a temperature range of 70 °C to 105 °C with a 5 K increment (Figure 6). DA-L0, DA-L40, and DA-L50 showed a clear decay of the modulus over time, reaching a relaxation modulus near zero at all temperatures. This means that even with lignin integrated, the network can completely relax the applied stresses, indicating the absence of a permanent network. Stress relaxation experiments on DA-L60 resulted in macroscopic phase separation and are therefore not included. For each network, the time required to reach a value of 1/e times the initial modulus is indicated on the graphs. In case of a single relaxation time decay, or a narrow monomodal relaxation time distribution, this time would correspond with the (average) relaxation time (τ). Comparing the results at 85 °C and 90 °C for the different materials, the time to reach a decay of

1/e is longer when lignin is present, indicating a slower relaxation when lignin is present. This can be attributed to the higher stiffness of the lignin-containing networks, due to their higher aromaticity and slightly higher crosslink density. As the networks are phase-separated at the 5-15 nm scale, a superposition of multiple relaxation times is expected. Indications for this are visible in figure 6b and c, where a clear kink in the relaxation decay is observed for DA-L40 and DA-L50 at 80 °C and 85°C, respectively. In DA-L0, the presence of two peaks in the tan(δ) from DMA (Figure 5c) also indicates the presence of a bimodal relaxation time distribution. The quantification of the complex relaxation time distributions for these networks and their time and temperature dependence is outside the scope of this work.

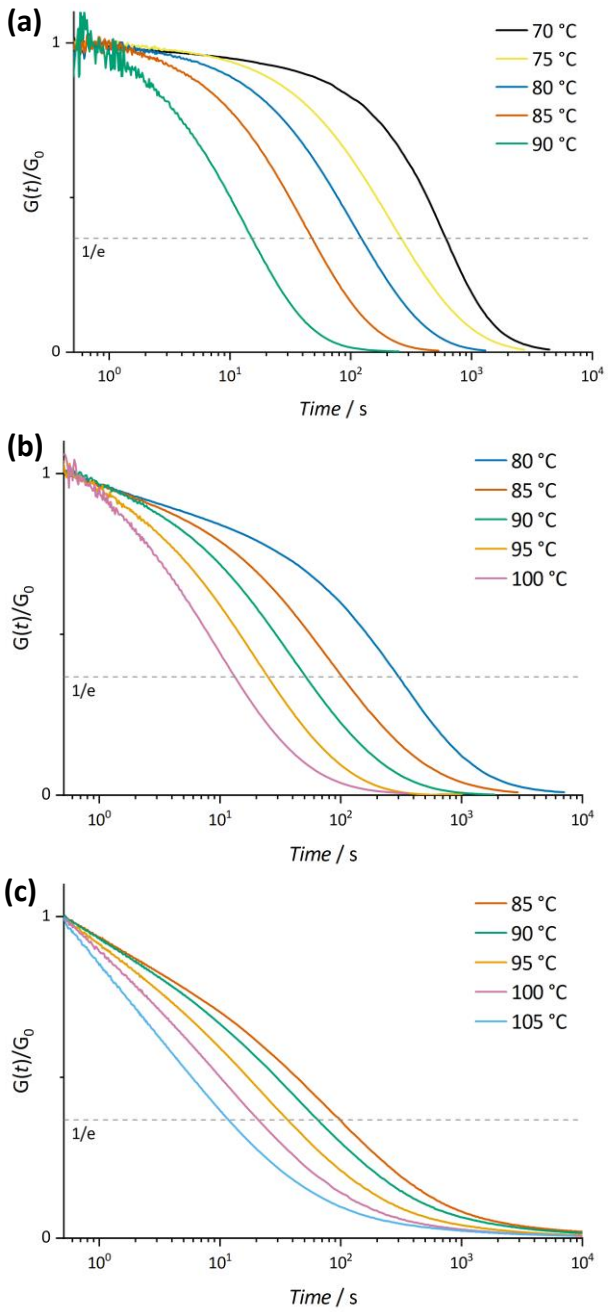

Figure 6. Normalized stress-relaxation data of a) DA-L0, b) DA-L40, and c) DA-L50. The relaxation time (τ) at each temperature is indicated by the grey dashed line (1/e).

Creep resistance of lignin-based network films. The suppression of creep is one of the main challenges in reversible polymer networks, as good healing efficiencies are often associated with

poor creep resistance and vice versa. In figure 7, the creep behavior at 25 °C and at an applied stress of 3 kPa is depicted for all networks. As expected, the reference network DA-L0 showed substantial creep behavior at a relatively short time scale (300 s). This indicates that the dynamic DA-equilibrium at 25 °C proceeds too fast under load to suppress creep. However, with increasing lignin content, the creep resistance under the same load increased. The increasing crosslink density combined with the presence of a fraction of the reversible groups in the vitrified state are thought to be the main reasons for the increased creep resistance, as this restricts the mobility of chains and suppresses creep. As a result, phase separation could have a significant impact on the creep resistance behavior in reversible networks.

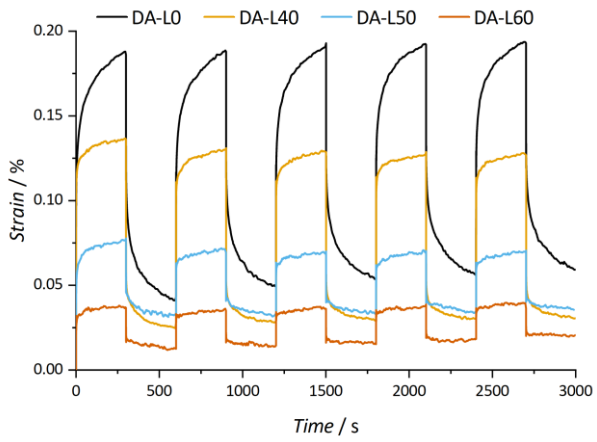

Figure 7. Creep of DA-L0, DA-L40, DA-L50, and DA-L60 at 25 °C temperature measured with an applied stress of 3 kPa.

Self-healing and reprocessing of lignin-based network films. The developed networks were tested on their healing capacity and reprocessing properties. Healing experiments were performed by pressing two pieces of a freshly cut network against each other at elevated temperatures, followed by controlled cooling (Figure S6). As the crosslink density of the networks increased

from DA-L0 towards DA-L60, different healing temperatures were applied to improve the mobility: the networks were healed at 85 °C, 120 °C, 125 °C and 130 °C for DA-L0, DA-L40, DA-L50 and DA-L60, respectively. These temperatures are below the (de)gelation temperature. In figure 8a, the stress-strain graphs of the healed networks are compared to the initial networks, showing promising healing behavior for DA-L0 and DA-L40 (Table 5). DA-L0 recovered its Young's modulus and stress at break, however, the strain at break decreased. In contrast, DA-L40 recovered its strain at break, while a lower Young's modulus and stress at break were observed after healing. These observations can be related to the temperature program used for the healing of the networks. DA-L0 and DA-L40 were healed at 85 °C and 120 °C, respectively. In both cases, the limiting factor to increase these healing temperatures further is the ability of these materials to flow at higher temperatures (melt viscosity measurements can be found in Figure S7). Once the material flows, the process cannot be described anymore as healing. In DA-L40, the healing is thus performed below the T_g of the lignin phase, which restricts efficient healing. As predominantly this lignin phase is responsible for the Young's modulus and stress at break, lower values are obtained. Nevertheless, at 120 °C the flexible F5000 phase, mainly responsible for the strain at break, recovered completely. Therefore, a promising healing efficiency (calculated by the toughness before and after healing) of 62 % was obtained (Table 5). DA-L50 was healed at 125 °C and showed full recovery of the Young's modulus, supporting the observations described above. However, the network failed rapidly due to an observable increase in brittleness after the healing program. Similarly, healed DA-L60 samples broke before the tensile test could even be started. It is hypothesized that radical initiated self-condensation of lignin during the healing program may contribute to this observation. It is known in literature that at temperatures above 130 °C, the phenolic OH of lignin can undergo a self-condensation reaction leading to a drastic

increase in molecular weight.[44,45] Although most of the phenolic OH groups are modified with FGE moieties, still roughly 11% phenolic OH groups might contribute to this side reaction. Optimization of the reaction conditions toward complete modification of the phenolic OH with FGE groups could possibly prevent lignin self-condensation and improve the thermal stability of lignin further. However, more research is necessary to fully understand the ongoing processes of lignin at elevated temperatures.

It is clear that the healing efficiencies decreased when the creep resistance was improved. For this series of materials, a compromise needs to be made between efficient healing and efficient creep resistance depending on the specific applications envisaged. Further research would need to be performed to overcome this problem in future self-healable materials.

The reprocessing of the networks was performed by dissolving the pre-tensile tested networks in chloroform at a concentration of 149 g/L at 55 °C (Figure S8). As the DA equilibrium is shifted towards dissociation by swelling and dilution, the network is gradually dissolved. After complete dissolution, the solutions were cast as described previously. Stress-strain curves were measured from the (re)processed networks and are depicted in figure 8b. In general, all networks show results equivalent to the ones of the original networks. Both DA-L0 and DA-L40 showed an improved strain at break, which both resulted in reprocessing efficiencies above 100 % (table 5). Probably the DA equilibrium reaction is the main reason for this observation. The initial networks were stored at ambient temperature for a longer period prior to analysis compared to the reprocessed analogues. Therefore, they had more time to equilibrate towards their most stable form, which could result in a higher crosslink density, and in turn, result in a lower strain at break. Reprocessed DA-L50 and DA-L60 show both a different trend compared to their initial networks. A difference in morphology of the phase-separated structure, cast from more dilute solutions, might explain this

change. Nevertheless, DA-L50 and DA-L60 also showed reprocessing efficiencies of more than 100 % (table 5).

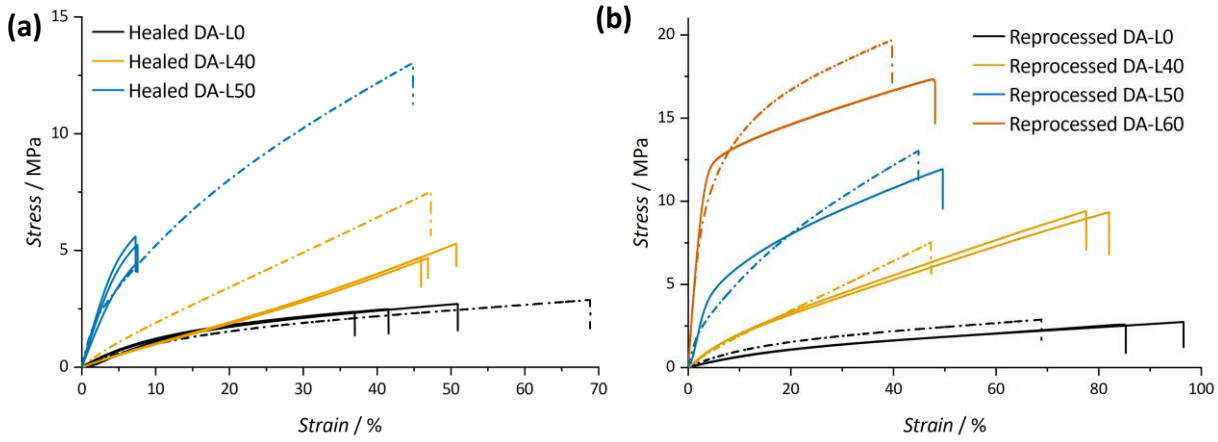

Figure 8. Stress-strain diagram (a) after fracture healing (b) after reprocessing. Dashed lines are the initial curves

Table 5. Mechanical data of the healed and reprocessed DA networks

		DA-L0	DA-L40	DA-L50	DA-L60
Healed network properties					
Young's Modulus	MPa	15 ± 1	12 ± 1	100 ± 7	-
Stress at break	MPa	2.5 ± 0.2	4.9 + 0.3	5.1 + 0.3	-
Strain at break	%	43 ± 3	48 ± 3	7.4 ± 0.4	-
Toughness	J m^{-3}	0.72 ± 0.08	1.1 ± 0.1	0.23 ± 0.03	-
Healing efficiency[a]	%	64	62	6	-
Reprocessed network properties					
Young's Modulus	MPa	6.9 ± 0.2	21 ± 1	125 ± 4	432 ± 12
Stress at break	MPa	2.7 ± 0.1	9.4 ± 0.1	12 ± 1	17 ± 1
Strain at break	%	91 ± 4	80 ± 4	50 ± 2	48 ± 2
Toughness	J m^{-3}	1.5 ± 0.1	4.2 ± 0.3	4.1 ± 0.3	7.0 ± 0.4
Reprocessing efficiency[a]	%	132	233	114	112

[a]Calculated by the toughness before healing divided by the toughness after healing

CONCLUSION

Ethyl methyl ketone (EMK)-extracted Kraft lignin was modified with furan moieties and was successfully integrated into a Diels-Alder network formulation combining a furan functional polyether (F5000) and a bismaleimide (DPBM). The extraction and modification of Kraft lignin resulted in a more compatible lignin fraction, which facilitated their incorporation into the Diels-Alder elastomers. The lignin incorporation had a significant effect on the thermal stability, possibly due to a combination of its aromatic nature and antioxidant properties. The final elastomers were phase-separated with domain sizes of the order of nm between a flexible F5000-rich phase and a rigid lignin-rich phase. This phase separation combined with the increasing crosslink densities has a significant impact on the mechanical properties. Especially the toughness increased six times for DA-L60 with 29 wt% of lignin compared to the reference material. In addition, the creep resistance improved, which is beneficial for application purposes. However, with the increased mechanical stability, the healing efficiencies decreased, which is probably related to restricted mobility of the reversible Diels-Alder adducts in the rigid lignin-rich phase. Therefore, a compromise still needs to be made between healing and creep/mechanical robustness to make these self-healing materials industrially viable. Nevertheless, besides the healing, the materials showed complete reprocessability by resolubilizing and recasting the networks, with full recovery of the toughness. This proves the complete reversibility of the networks and results in promising recycling options. Although the use of solvents is not ideal for large-scale applications, other reprocessing techniques could be investigated in the future, such as remolding, extrusion, or even 3D printing.

ASSOCIATED CONTENT

Supporting Information: Supporting characterization methods, furan-functionality calculations, pooled standard error calculations, ^{31}P-NMR spectra, DSC thermograms, FT-IR spectra of modified/EMK extracted Kraft lignin, SAXS spectra, MTDSC spectra of 100% lignin network, melt viscosity measurements, healing process, and reprocessing process.

AUTHOR INFORMATION

Corresponding Author

*E-mail: Richard.vendamme@vito.be, Niko.Van.den.Brande@vub.be

ORCID

Marlies Thys: 0000-0003-0568-7457

Joost Brancart: 0000-0002-1735-1515

Guy Van Assche: 0000-0003-0452-6272

Richard Vendamme: 0000-0002-8931-0851

Niko Van den Brande: 0000-0002-5324-6261

Notes

The authors declare no competing financial interest

ACKNOWLEDGMENT

The authors would like to thank Innventia Institute for providing Lignoboost® Kraft lignin, Brigitte Lamers from the Meijers research group at Tu/e for measuring the SAXS spectra, and The Research Foundation - Flanders for the Ph.D. fellowship of Marlies Thys (1SA8620N) and for the Junior postdoctoral fellowship of Joost Brancart (12W4719N).

REFERENCES

(1) Skoczinski, P.; Chinthapalli, R.; Carus, M.; Baltus, W.; de Guzman, D.; Käb, H.; Raschka, A.; Ravenstijn, J. *Bio-based Building Blocks and Polymers – Global Capacities, Production and Trends 2019 – 2024*; nova-Institut GmbH, 2020;

(2) Lin, Z.; Nikolakis, V.; Ierapetritou, M. Alternative approaches for p-xylene production from starch: Techno-economic analysis. *Ind. Eng. Chem. Res.* **2014**, *53*, 10688–10699. DOI: 10.1021/ie402469j.

(3) Ten, E.; Vermerris, W. Recent developments in polymers derived from industrial lignin. *J. Appl. Polym. Sci.* **2015**, *132*, 1–13. DOI: 10.1002/app.42069.

(4) Wallberg, O.; Jönsson, A.-S.; Wimmerstedt, R. Fractionation and concentration of kraft black liquor lignin with ultrafiltration. *Desalination* **2003**, *154*, 187–199. DOI: 10.1016/S0011-9164(03)80019-X.

(5) Toledano, A.; García, A.; Mondragon, I.; Labidi, J. Lignin separation and fractionation by

ultrafiltration. *Sep. Purif. Technol.* **2010**, *71*, 38–43. DOI: 10.1016/j.seppur.2009.10.024.

(6) Sevastyanova, O.; Helander, M.; Chowdhury, S.; Lange, H.; Wedin, H.; Zhang, L.; Ek, M.; Kadla, J.F.; Crestini, C.; Lindstr, M.E. Tailoring the Molecular and Thermo – Mechanical Properties of Kraft Lignin by Ultrafiltration. *J. Appl. Polym. Sci.* **2014**, *40799*, 1–11. DOI: 10.1002/app.40799.

(7) Duval, A.; Vilaplana, F.; Crestini, C.; Lawoko, M. Solvent screening for the fractionation of industrial kraft lignin. *Holzforschung* **2015**, *70*, 11–20. DOI: 10.1515/hf-2014-0346.

(8) Passoni, V.; Scarica, C.; Levi, M.; Turri, S.; Gri, G. Fractionation of Industrial Softwood Kraft Lignin: Solvent Selection as a Tool for Tailored Material Properties. *ACS Sustain. Chem. Eng.* **2016**, *4*, 2232–2242. DOI: 10.1021/acssuschemeng.5b01722.

(9) Wang, Y.Y.; Li, M.; Wyman, C.E.; Cai, C.M.; Ragauskas, A.J. Fast Fractionation of Technical Lignins by Organic Cosolvents. *ACS Sustain. Chem. Eng.* **2018**, *6*, 6064–6072. DOI: 10.1021/acssuschemeng.7b04546.

(10) Saito, T.; Perkins, J.H.; Vautard, F.; Meyer, H.M.; Messman, J.M.; Tolnai, B.; Naskar, A.K. Methanol fractionation of softwood Kraft lignin: Impact on the lignin properties. *ChemSusChem* **2014**, *7*, 221–228. DOI: 10.1002/cssc.201300509.

(11) Gioia, C.; Lo Re, G.; Lawoko, M.; Berglund, L. Tunable Thermosetting Epoxies Based on Fractionated and Well-Characterized Lignins. *J. Am. Chem. Soc.* **2018**, *140*, 4054–4061. DOI: 10.1021/jacs.7b13620.

(12) Ortiz, P.; Vendamme, R.; Eevers, W. Fully biobased epoxy resins from fatty acids and lignin. *Molecules* **2020**, *25*, 1–11. DOI: 10.3390/molecules25051158.

(13) Yoshida, H.; Mörck, R.; Kringstad, K.P.; Hatakeyama, H. Kraft lignin in polyurethanes. II. Effects of the molecular weight of kraft lignin on the properties of polyurethanes from a kraft lignin–polyether triol–polymeric MDI system. *J. Appl. Polym. Sci.* **1990**, *40*, 1819–1832. DOI: 10.1002/app.1990.070401102.

(14) Vanderlaan, M.N.; Thring, R.W. Polyurethanes from Alcell® lignin fractions obtained by sequential solvent extraction. *Biomass and Bioenergy* **1998**, *14*, 525–531. DOI: 10.1016/S0961-9534(97)10058-7.

(15) Vendamme, R.; Behaghel De Bueren, J.; Gracia-Vitoria, J.; Isnard, F.; Mulunda, M.M.; Ortiz, P.; Wadekar, M.; Vanbroekhoven, K.; Wegmann, C.; Buser, R.; et al. Aldehyde-Assisted Lignocellulose Fractionation Provides Unique Lignin Oligomers for the Design of Tunable Polyurethane Bioresins. *Biomacromolecules* **2020**, *21*, 4135–4148. DOI: 10.1021/acs.biomac.0c00927.

(16) Griffini, G.; Passoni, V.; Suriano, R.; Levi, M.; Turri, S. Polyurethane coatings based on chemically unmodified fractionated lignin. *ACS Sustain. Chem. Eng.* **2015**, *3*, 1145–1154. DOI: 10.1021/acssuschemeng.5b00073.

(17) De Haro, J.C.; Allegretti, C.; Smit, A.T.; Turri, S.; D'Arrigo, P.; Griffini, G. Biobased Polyurethane Coatings with High Biomass Content: Tailored Properties by Lignin Selection. *ACS Sustain. Chem. Eng.* **2019**, *7*, 11700–11711. DOI: 10.1021/acssuschemeng.9b01873.

(18) Wang, L.; Lagerquist, L.; Zhang, Y.; Koppolu, R.; Tirri, T.; Sulaeva, I.; Schoultz, S. von; Vähäsalo, L.; Pranovich, A.; Rosenau, T.; et al. Tailored Thermosetting Wood Adhesive Based on Well-Defined Hardwood Lignin Fractions. *ACS Sustain. Chem. Eng.* **2020**, *8*,

13517–13526. DOI: 10.1021/acssuschemeng.0c05408.

(19) Hager, M.D. Self-healing Materials. In *Handbook of Solid State Chemistry*; Wiley-VCH Verlag GmbH & Co. KGaA: Weinheim, Germany, 2017; pp. 201–225. DOI: 10.1002/9783527691036.hsscvol6016.

(20) Winne, J.M.; Leibler, L.; Du Prez, F.E. Dynamic covalent chemistry in polymer networks: A mechanistic perspective. *Polym. Chem.* **2019**, *10*, 6091–6108. DOI: 10.1039/c9py01260e.

(21) Kloxin, C.J.; Bowman, C.N. Covalent adaptable networks: Smart, reconfigurable and responsive network systems. *Chem. Soc. Rev.* **2013**, *42*, 7161–7173. DOI: 10.1039/c3cs60046g.

(22) McBride, M.K.; Worrell, B.T.; Brown, T.; Cox, L.M.; Sowan, N.; Wang, C.; Podgorski, M.; Martinez, A.M.; Bowman, C.N. Enabling applications of covalent adaptable networks. *Annu. Rev. Chem. Biomol. Eng.* **2019**, *10*, 175–198. DOI: 10.1146/annurev-chembioeng-060718-030217.

(23) Chen, X.; Dam, M.A.; Ono, K.; Mal, A.; Shen, H.; Nutt, S.R.; Sheran, K.; Wudl, F. A thermally re-mendable cross-linked polymeric material. *Science (80-.).* **2002**, *295*, 1698–1702. DOI: 10.1126/science.1065879.

(24) Scheltjens, G.; Brancart, J.; De Graeve, I.; Van Mele, B.; Terryn, H.; Van Assche, G. Self-healing property characterization of reversible thermoset coatings. *J. Therm. Anal. Calorim.* **2011**, *105*, 805–809. DOI: 10.1007/s10973-011-1381-4.

(25) Ehrhardt, D.; Mangialetto, J.; Bertouille, J.; Van Durme, K.; Van Mele, B.; Van den Brande,

N. Self-healing in mobility-restricted conditions maintaining mechanical robustness: Furan–maleimide diels–alder cycloadditions in polymer networks for ambient applications. *Polymers (Basel).* **2020**, *12*, 1–24. DOI: 10.3390/polym12112543.

(26) Ehrhardt, D.; Van Durme, K.; Jansen, J.F.G.A.; Van Mele, B.; Van den Brande, N. Self-healing UV-curable polymer network with reversible Diels-Alder bonds for applications in ambient conditions. *Polymer (Guildf).* **2020**, *203*, 122762. DOI: 10.1016/j.polymer.2020.122762.

(27) Mangialetto, J.; Cuvellier, A.; Verhelle, R.; Brancart, J.; Rahier, H.; Van Assche, G.; Van Den Brande, N.; Van Mele, B. Diffusion- and Mobility-Controlled Self-Healing Polymer Networks with Dynamic Covalent Bonding. *Macromolecules* **2019**, *52*, 8440–8452. DOI: 10.1021/acs.macromol.9b01453.

(28) Peterson, A.M.; Jensen, R.E.; Palmese, G.R. Room-temperature healing of a thermosetting polymer using the diels-alder reaction. *ACS Appl. Mater. Interfaces* **2010**, *2*, 1141–1149. DOI: 10.1021/am9009378.

(29) Duval, A.; Lange, H.; Lawoko, M.; Crestini, C. Reversible crosslinking of lignin via the furan-maleimide Diels-Alder reaction. *Green Chem.* **2015**, *17*, 4991–5000. DOI: 10.1039/C5GC01319D.

(30) Zhou, W.; Zhang, H.; Chen, F. Modified lignin: Preparation and use in reversible gel via Diels-Alder reaction. *Int. J. Biol. Macromol.* **2018**, *107*, 790–795. DOI: 10.1016/j.ijbiomac.2017.09.052.

(31) Buono, P.; Duval, A.; Averous, L.; Habibi, Y. Thermally healable and remendable lignin-

based materials through Diels – Alder click polymerization. *Polymer (Guildf).* **2017**, *133*, 78–88. DOI: 10.1016/j.polymer.2017.11.022.

(32) Scheltjens, G.; Diaz, M.M.; Brancart, J.; Van Assche, G.; Van Mele, B. A self-healing polymer network based on reversible covalent bonding. *React. Funct. Polym.* **2013**, *73*, 413–420. DOI: 10.1016/j.reactfunctpolym.2012.06.017.

(33) Brancart, J.; Scheltjens, G.; Muselle, T.; Van Mele, B.; Terryn, H.; Van Assche, G. Atomic force microscopy – based study of self-healing coatings based on reversible polymer network systems. *J. Intell. Mater. Syst. Struct.* **2014**, *25*, 40–46. DOI: 10.1177/1045389X12457100.

(34) Cui, C.; Sun, R.; Argyropoulos, D.S. Fractional precipitation of softwood kraft lignin: Isolation of narrow fractions common to a variety of lignins. *ACS Sustain. Chem. Eng.* **2014**, *2*, 959–968. DOI: 10.1021/sc400545d.

(35) Brodin, I.; Sjöholm, E.; Gellerstedt, G. Kraft lignin as feedstock for chemical products: The effects of membrane filtration. *Holzforschung* **2009**, *63*, 290–297. DOI: 10.1515/HF.2009.049.

(36) Kubo, S.; Kadla, J.F. Hydrogen bonding in lignin: A fourier transform infrared model compound study. *Biomacromolecules* **2005**, *6*, 2815–2821. DOI: 10.1021/bm050288q.

(37) Brancart, J.; Verhelle, R.; Mangialetto, J.; Van Assche, G. Coupling the Microscopic Healing Behaviour of Coatings to the Thermoreversible Diels-Alder. *Coatings* **2019**, *9*, 13. DOI: 10.3390/coatings9010013.

(38) Sadeghifar, H.; Argyropoulos, D.S. Correlations of the antioxidant properties of softwood

kraft lignin fractions with the thermal stability of its blends with polyethylene. *ACS Sustain. Chem. Eng.* **2015**, *3*, 349–356. DOI: 10.1021/sc500756n.

(39) Canetti, M.; Bertini, F.; De Chirico, A.; Audisio, G. Thermal degradation behaviour of isotactic polypropylene blended with lignin. *Polym. Degrad. Stab.* **2006**, *91*, 494–498. DOI: 10.1016/j.polymdegradstab.2005.01.052.

(40) Lartigue-Peyrou, F. The use of phenolic compounds as free-radical polymerization inhibitors. *Ind. Chem. Libr.* **1996**, *8*, 489–505. DOI: 10.1016/S0926-9614(96)80036-0.

(41) Horrocks, A.R. Developments in flame retardants for heat and fire resistant textiles - The role of char formation and intumescence. *Polym. Degrad. Stab.* **1996**, *54*, 143–154. DOI: 10.1016/s0141-3910(96)00038-9.

(42) Cuvellier, A.; Verhelle, R.; Brancart, J.; Vanderborght, B.; Van Assche, G.; Rahier, H. The influence of stereochemistry on the reactivity of the Diels-Alder cycloaddition and the implications for reversible network polymerization. *Polym. Chem.* **2019**, *10*, 473–485. DOI: 10.1039/c8py01216d.

(43) Diaz, M.M.; Van Assche, G.; Maurer, F.H.J.; Van Mele, B. Thermophysical characterization of a reversible dynamic polymer network based on kinetics and equilibrium of an amorphous furan-maleimide Diels-Alder cycloaddition. *Polymer (Guildf).* **2017**, *120*, 176–188. DOI: 10.1016/j.polymer.2017.05.058.

(44) Cui, C.; Sadeghifar, H.; Sen, S.; Argyropoulos, D.S. Toward thermoplastic lignin polymers; Part II: Thermal & polymer characteristics of kraft lignin & derivatives. *BioResources* **2013**, *8*, 864–886. DOI: 10.15376/biores.8.1.864-886.

(45) Sen, S.; Patil, S.; Argyropoulos, D.S. Methylation of softwood kraft lignin with dimethyl carbonate. *Green Chem.* **2015**, *17*, 1077–1087. DOI: 10.1039/c4gc01759e.